Energy & Environmental Science

COMMUNICATION

View Article Online
View Journal | View Issue

Cite this: *Energy Environ. Sci.*, 2016, **9**, 2037

Received 24th February 2016,
Accepted 28th April 2016

DOI: 10.1039/c6ee00587j

www.rsc.org/ees

11.3% efficiency Cu(In,Ga)(S,Se)$_2$ thin film solar cells *via* drop-on-demand inkjet printing†

Xianzhong Lin,*[a] Reiner Klenk,[a] Lan Wang,[a] Tristan Köhler,[a] Jürgen Albert,[a] Sebastian Fiechter,[a] Ahmed Ennaoui[ab] and Martha Ch. Lux-Steiner[ac]

Although Cu(In,Ga)(S,Se)$_2$ (CIGSe) based thin film solar cells have reached efficiencies exceeding 22% based on vacuum processed CIGSSe absorbers, the supply of indium and gallium might become an issue if CIGSSe thin-film solar cells are produced in very large volumes. It is therefore mandatory to reduce the wastage of indium and gallium during the fabrication process. In this work, we report on a highly efficient precursor utilization, and a vacuum-free, and scalable route to the deposition of Cu(In,Ga)(S,Se)$_2$ (CIGSSe) thin films *via* drop-on-demand inkjet-printing. The precursor ink, which shows long-term stability in air at room temperature, is formulated by dissolving metal nitrate salts in alcohol-based solvents. Crack free CIGSSe absorbers consisting of a layer with large grains at the surface and a layer with small grains at the back have been prepared by annealing the inkjet-printed Cu–In–Ga nitrate precursors in a Se/H_2S containing atmosphere. Ga accumulation has been observed within the layer with small grains. A solar cell with a total area efficiency of 11.3% under standard AM 1.5 illumination has been achieved based on the printed CIGSSe absorbers.

Broader context

Among all the thin film solar cell technologies developed so far, Cu(In,Ga)Se$_2$-based thin film solar cells exhibit the best performance with an efficiency of 22.3%. The main challenge in the widespread application of solar cells is to reduce the cost in order to compete with conventional energy sources. It is believed that one way to reduce the cost is to use a solution process for the fabrication of solar cells, which does not rely on a high cost vacuum-based facility but has high raw material utilization. As one of the solution process based methods, drop-on-demand inkjet printing shows remarkable advantages such as high efficiency in terms of precursor utilization and easy adaptability to roll-to-roll processes for high throughput production. One could expect that one day solar cells can be produced using a similar process to that used in the printing of newspapers showing a significant cost reduction compared to the conventional vacuum-based process. In this work, we report the fabrication of Cu(In,Ga)(S,Se)$_2$ solar cells with total area efficiencies exceeding 11% using the drop-on-demand inkjet printing technology based on air stable Cu–In–Ga nitrate inks. These encouraging results are a first indication that the unique advantages of air-stable inks and inkjet printing can be exploited without sacrificing device performance.

Cu(In,Ga)Se$_2$ (CIGSe) thin film solar cells have reached conversion efficiencies of over 22%. Although crystalline Si-based solar cells have reached efficiencies of over 25%,[1] CIGSSe solar cells are nevertheless of great interest due to unique advantages of their thin films.[2,3] Si-based solar cells are dominating the market. To compete with them, the development of solar cells with high efficiency at low production cost is essential. So far, the best performing CIGSSe solar cells rely on high vacuum processes (three stage evaporation yielding an efficiency of 21.7%[4] and reactive annealing of sputtered metal precursors yielding 22.3%[5]). It is believed that one of the ways to reduce the production cost is to use solution processes, in particular the printing process, to fabricate solar cells.[6–8] Many groups have been working on different methods such as spin coating,[9–13] doctor blading[14–18] and spraying,[19–21] which are all based on either nanoparticle or molecular ink precursors. The best solar cell based on a solution process has an efficiency of 15.2% as reported by Todorov *et al.* who fabricated the CIGSSe absorbers by using a hydrazine-based solution process.[11] Using hydrazine as a solvent is undesirable for mass production due to its toxic and explosive properties. Therefore, alternative inks should be formulated in order to facilitate mass production. Recently, Uhl *et al.* reported a route for the formulation of Cu–In–Ga–S ink by forming Cu-thiourea-chloride, In-dimethyl sulfoxide-chloride and Ga-dimethyl sulfoxide–chloride in a dimethyl sulfoxide solvent.[12] The achieved power conversion efficiencies of CIGSSe solar cells prepared from this ink have reached as high as 14.7%, which is quite promising. However, there are some limitations in terms of the ink formulation process and stability of the ink in this process. On the one hand, the ink formulation process is

[a] *Helmholtz-Zentrum Berlin für Materialien und Energie, Hahn-Meitner-Platz 1, D-14109 Berlin, Germany. E-mail: lin.xianzhong@helmholtz-berlin.de*
[b] *Qatar Environment and Energy Research Institute and College of Science and Engineering (CSE), Hamad Bin Khalifa University, Education City, Doha, Qatar*
[c] *Freie Universität Berlin, Fachbereich Physik, Arnimallee 14, 14195 Berlin, Germany*

† Electronic supplementary information (ESI) available. See DOI: 10.1039/c6ee00587j

performed inside a glovebox, and in order to form the complex a heating step to 120 °C is required, which is rather complex. Therefore, an air stable simpler process is preferred in order to facilitate industrial production. On the other hand, both of these two best results are based on the spin coating method which has low efficiency in terms of raw material utilization.

Considering the expensive indium and gallium constituents, one way to reduce the cost of CIGSSe solar cells is to reduce the wastage of indium and gallium during the absorber production process. This is also important considering that the supply of these metals might become an issue once CIGSe thin-film solar cells are produced in very large volumes (70 GW per year).[22] In this context, the drop-on-demand inkjet printing approach has intrinsic advantages. It is a solution-based technique, which does not rely on high vacuum for precursor deposition. Additionally, compared to the conventional solution deposition methods, *i.e.* spin coating, this technique can significantly increase the raw material utilization due to its drop-on-demand feature. For instance, less than 25 μL of the precursor ink is required to deposit the precursor for a 1 μm thick CIGSSe absorber on an inch by inch substrate *via* the inkjet-printing technique, while at least 100 μL is needed for one spin coating with a thickness of 200–300 nm. Nearly all the precursor inks can be utilized due to the drop-on-demand property of inkjet-printing. Another great advantage of inkjet printing is that it can be easily adapted to roll-to-roll processes for mass production. This technology has attracted considerable attention from both scientific and industrial research communities due to its unique properties. So far, the highest power conversion efficiency of an inkjet-printed CIGSSe solar cell is 5.04% as reported by Wang *et al.*,[23] where the ink was formulated by dissolving copper acetate, indium acetate and gallium chloride in a mixture solvent of ethanol, ethylene glycol and ethanolamine. Previously, we have demonstrated that the inkjet printing technology can also be applied to the fabrication of kesterite absorbers and indium sulfide buffers.[24–26] In this communication, we exploit the application of this technology to the preparation of CIGSSe solar cells. We have developed a simple route for the formulation of a printable Cu–In–Ga ink by mixing Cu, In, and Ga nitrates in alcohol-based solvents at room temperature. This ink shows long-term stability in air. A power conversion efficiency exceeding 11% has been demonstrated for a CIGSSe solar cell based on inkjet-printed precursors using this air-stable Cu–In–Ga ink.

Fig. 1(a) shows a photograph of the ink with a clear blue color. The wetting behaviour between the ink and the substrate plays an important role in the formation of homogeneous films. One way to examine this is to measure the contact angle of the ink on the substrate. Therefore, we first checked the contact angle of the Cu–In–Ga ink on Mo coated soda lime glass. As shown in Fig. 1(b), the contact angle is 27°, which is even smaller than that of our previous Cu–Zn–Sn–S ink,[24] indicating that wetting is suitable for printing.[27,28]

It is known that metal nitrate compounds are easily decomposed into the corresponding metal oxides by heating up to certain temperatures.[29–31] Here, thermogravimetric analysis (TGA) has been utilized to study the thermal decomposition

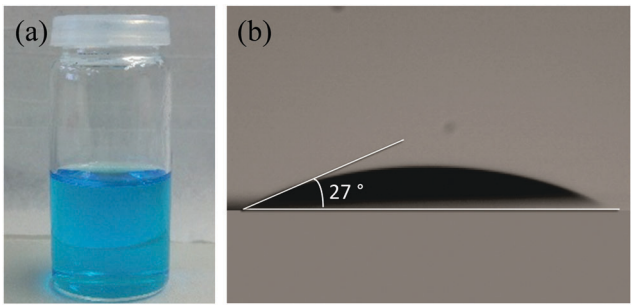

Fig. 1 (a) Photograph of the molecular Cu–In–Ga ink and (b) contact angle between the molecular ink and a Mo coated glass substrate.

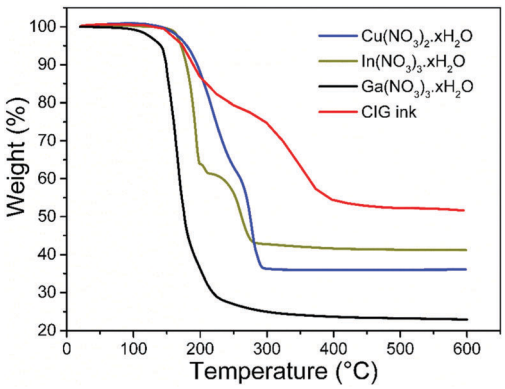

Fig. 2 Thermogravimetric analysis (TGA) of $Cu(NO_3)_2{\cdot}xH_2O$, $In(NO_3)_3{\cdot}xH_2O$, $Ga(NO_3)_3{\cdot}xH_2O$ precursors and the Cu–In–Ga precursor ink dried under vacuum at 80 °C.

of the individual metal nitrate precursors as well as the formulated ink during the thermal treatment process (Fig. 2). The TGA study of the pure metal nitrates indicates dehydration and decomposition stages, which together result in the corresponding metal oxides (CuO, In_2O_3 and Ga_2O_3). $Ga(NO_3)_3$ shows the lowest decomposition temperature while $Cu(NO_3)_2$ shows the highest. However, the decomposition of all individual compounds is nearly complete when the temperature reaches 300 °C with a ramping rate of 10 °C min^{-1}. The red curve in Fig. 2 represents the TGA curve of the precursor ink which was dried under vacuum at 80 °C before loading into a ceramic crucible for TGA measurements. The initial weight loss observed from room temperature to 300 °C is attributed to the evaporation of residual solvents as well as the decomposition of metal salt precursors into metal oxides. In principle, the decomposition should be completed at 300 °C according to the TGA analysis of the single metal nitrate precursors. However, there is a second significant mass loss between 300 and 400 °C, which is presumably related to the ethylene glycol solvent. Assuming that all the dried precursors are anhydrous, the products after decomposition should be CuO, In_2O_3 and Ga_2O_3, which should account for around 43% of the remaining mass. However, here the final mass is around 51%, indicating the contribution of other compounds. On the other hand, assuming that all the anhydrous precursors are metal ethylene glycol complexes such as $Cu(OCH_2CH_2O)$, $In_2(OCH_2CH_2O)_3$,

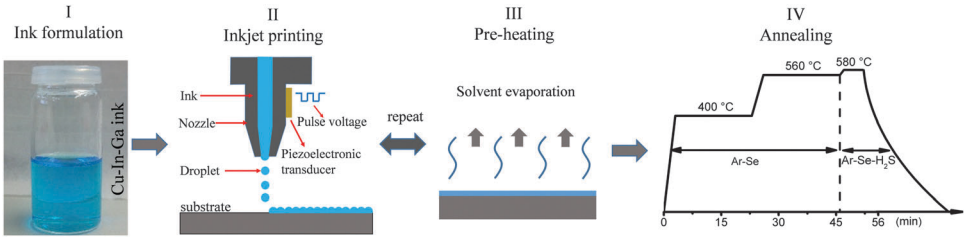

Scheme 1 Formation procedures of CIGSSe thin films consisting of four steps.

and $Ga_2(OCH_2CH_2O)_3$, the maximum remaining mass should be approximately 65%. The actual value of 51% is between 43% and 65%. Therefore, we speculate that this is due to the decomposition of metal nitrates as well as metal ethylene glycol complexes formed from the metal nitrates and the ethylene glycol solvent during the ink formulation process. Further study is required to fully understand this issue. Based on the TGA results, an extra intermediate step at 400 °C is to ensure the decomposition of the precursors before reaching the higher temperature annealing steps (Scheme 1).

Fig. 3 shows the GIXRD pattern of a completed CIGSSe solar cell. The most intensive peak located at 26.806° corresponds to the CIGSSe 112 plane, which is at a slightly larger angle than the 112 peak of pure $CuInSe_2$ at 26.572°. The diffraction peak position is shifted to a higher angle when replacing In with Ga and/or replacing Se with S due to the smaller atomic diameter. For instance, the 112 peak position is at 27.88° for pure $CuInS_2$ and at 27.769° for pure $CuGaSe_2$. The small difference of the 112 peak position between the CIGSSe sample and pure $CuInSe_2$ suggests that the sample contains only small amounts of Ga and/or S. The other less pronounced peaks related to CIGSSe such as 101, 211, 220/204 and 116/312 are also observed, as labeled in the figure. Since the XRD measurements have been performed on the solar cell sample, the peaks corresponding to the ZnO window layer, aluminum grid, indium contact and Mo substrate are also detected. XRD is insufficient to distinguish whether the shift of the peak to a higher angle is due to the incorporation of Ga or S in the $CuInSe_2$ absorbers. However, Raman spectroscopy can be used to identify the vibrational modes related to Se or S, respectively. As shown in Fig. 3(right), the dominating peak is at 176 cm^{-1}, which can be ascribed to the $CuInSe_2$-like A1 mode representing the vibrations of Se anions with cations (Cu, In, and Ga) at rest.[32] This frequency is slightly blue-shifted compared to the A1 mode of pure $CuInSe_2$ (173–174 cm^{-1}), which is due to the incorporation of Ga and S in the absorber layers.[32,33] Weaker bands at 213 cm^{-1} and 227 cm^{-1} are also observed, which can be attributed to the $CuInSe_2$-like B2/E modes. Since H_2S is applied during the last step during the annealing process, the incorporation of sulfur atoms into the absorbers forming CIGSSe is also evidenced by a weak Raman shift at 293 cm^{-1} attributed to the A1 mode of $CuInS_2$. Hence, both XRD and Raman confirm the formation of CIGSSe by annealing the printed Cu–In–Ga layers. Based on the results of TGA, XRD and Raman analyses, the formation of the CIGSSe can be expressed by the following chemical reactions: firstly, the metal nitrates or metal ethylene glycol complexes decompose into the corresponding oxides during the pre-heating and 400 °C annealing step. Secondly, the metal oxides react with selenium vapor at 560 °C forming a CIGSSe compound. And the last step is the partial replacement of Se in CIGSSe with S resulting in the formation of $Cu(In,Ga)(S,Se)_2$ when flowed with H_2S at 580 °C.

$$Cu(NO_3)_2, In(NO_3)_3, Ga(NO_3)_3 \xrightarrow{\Delta} CuO, In_2O_3, Ga_2O_3 \quad (1)$$

$$CuO + In_2O_3 + Ga_2O_3 \overset{Se,\Delta}{\Rightarrow} Cu(In,Ga)Se_2 \quad (2)$$

$$Cu(In,Ga)Se_2 \overset{H_2S,\Delta}{\Rightarrow} Cu(In,Ga)(S,Se)_2 \quad (3)$$

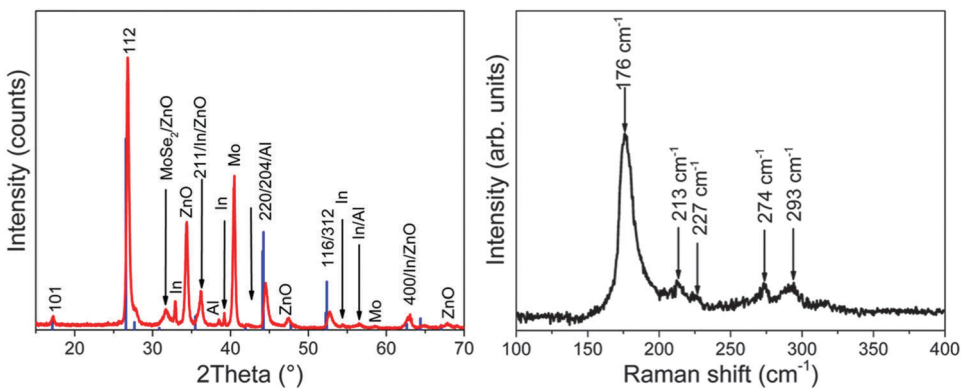

Fig. 3 XRD pattern (left) and Raman spectrum (right) of the CIGSSe solar cell sample. For comparison, the standard JCPDS card 40-1487 of $CuInSe_2$ is also shown in blue together with the experimental data.

Fig. 4 shows cross-sectional SEM images together with the Energy Dispersive X-ray (EDX) line scanning profile of a cross-section of the CIGSSe film. The inkjet-printed Cu–In–Ga layers after pre-heating appear uniform and compact with a thickness of around 1 μm (see Fig. 4(a)). Fig. 4(b) shows the cross-sectional image of a complete CIGSSe solar cell with the Mo/CIGSe/CdS/i-ZnO/Al:ZnO structure. The CIGSSe absorber shows a double-layer structure with an approximately 0.63 μm thick layer with large grains on top of a 0.33 μm layer with smaller grains at the back contact. A thin $MoSe_2$ layer (around 0.2 μm thick) can also be observed. This layered structure is common for solution processed CIGSSe and $Cu_2ZnSn(S,Se)_4$ thin films. Although McLeod *et al.* have demonstrated CIGSSe solar cells with 15% efficiency based on a nanoparticle ink route, there still is a fine grained layer underneath the large grained layer.[14] A layered structure was observed in both our nanoparticle ink based and molecular ink based inkjet-printed kesterite CZTSSe absorber thin films.[24,34] The reason for the formation of the layered structure is not completely clear, but residual carbon in the fine grained layer stemming from the organic solvents/surfactants in the precursor inks may play a role.[35,36] To study the elemental distribution through the depth of the CIGSSe absorbers, EDX analysis was performed. Fig. 4(c) displays the elements Cu, In, Ga and Se according to the EDX line scanning profile across the cross-section. Due the overlapping of S Kα with the Mo Lα signal, neither of these two elements is shown here. The concentrations of Cu and Se are nearly constant throughout the CIGSSe layer with a slight decrease of Cu and increase of Se within the small grained layer. The strong increase of Se near the back contact is due to the existence of $MoSe_2$ as shown in Fig. 4(b). The whole CIGSSe layer is mostly Cu-poor with the In concentration gradually dropping from the surface towards the back contact while the Ga concentration showing the opposite trend. Note that there is almost no Ga at the surface of the large grained CIGSSe layer. However, the Ga concentration dramatically increases in the fine grained layer. Assuming a certain degree of sulfur incorporation, the surface of the large grains is close to pure $CuIn(S,Se)_2$ while in the fine grained layer the composition is closer to $Cu(In,Ga)(S,Se)_2$. The overall ratio of Cu : In : Ga : Se is 1 : 1.3 : 0.2 : 2.1 as estimated from the EDX measurements, which is Cu-poor and In-rich.

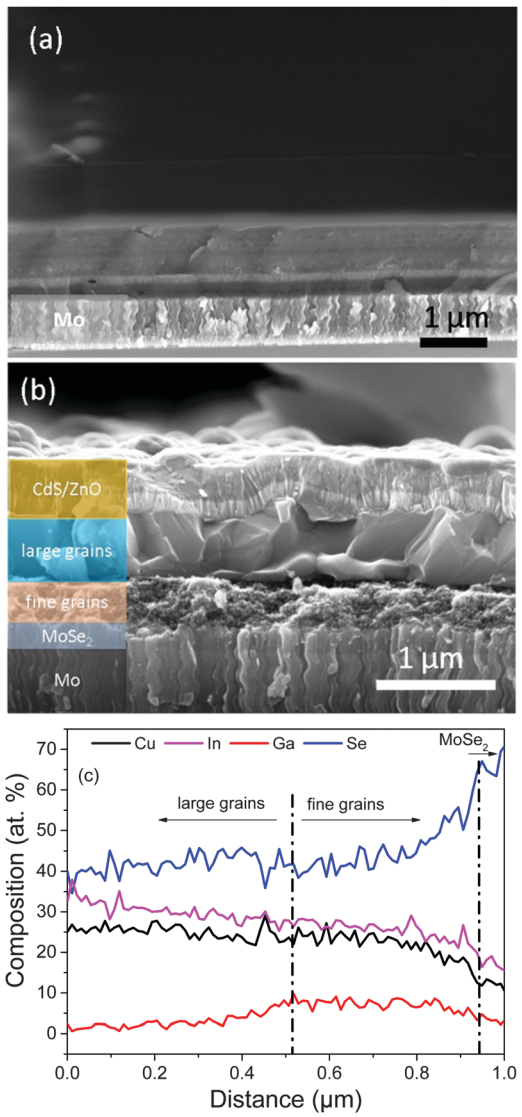

Fig. 4 Cross-sectional SEM images of a pre-heated Cu–In–Ga precursor (a) and of the best solar cell with an annealed CIGSSe thin film (b). The EDX line scanning profile corresponding to (b) is shown in (c).

The solar cells were completed by the deposition a CdS buffer layer, i-ZnO/ ZnO:Al window layers, and Ni/Al grids. The typical *I–V* curves and device parameters of the best devices are shown in Fig. 5(a). A solar cell with a total area efficiency of 11.3% was achieved, with an open circuit voltage (V_{OC}) of 541 mV, short circuit current density (J_{SC}) of 31.1 mA cm^{-2}, and fill factor (FF) of 67.0%. The maximum external quantum efficiency (EQE) reaches up to 90%, suggesting nearly loss free collection of light generated charge carriers at that wavelength suggesting good carrier lifetimes at the interface and in the upper part of the absorber. However, the near infrared response shown by the EQE is poor. In general, several reasons can contribute to the poor red response: rear surface (back contact) recombination, insufficient light absorption and low diffusion length.[37] Wu *et al.* performed a comprehensive study on the effect of the fine-grain layer and suggested that it does not contribute to the photo-response of the $Cu_2ZnSn(S,Se)_4$ photovoltaic device.[35] Here, assuming that current is mainly collected from the large grained layer, the effective thickness of the CIGSSe absorber is only around 600 nm which would not be thick enough to absorb all the light. We therefore suspect that a combination of insufficient light absorption in the upper layer and failure to collect carriers from the lower layer could be the main reason for the poor red response in our case. To support our assumption, SCAPS[38] simulation of the quantum efficiency with different absorber thicknesses was performed. Assuming the same diffusion length, the red response decreases as expected when the absorber thickness is reduced due to the insufficient light absorption. Particularly, when the absorber thickness is less than 500 nm, this behavior is very pronounced (see the ESI,† Fig. S2). Comparing the slopes of the measured

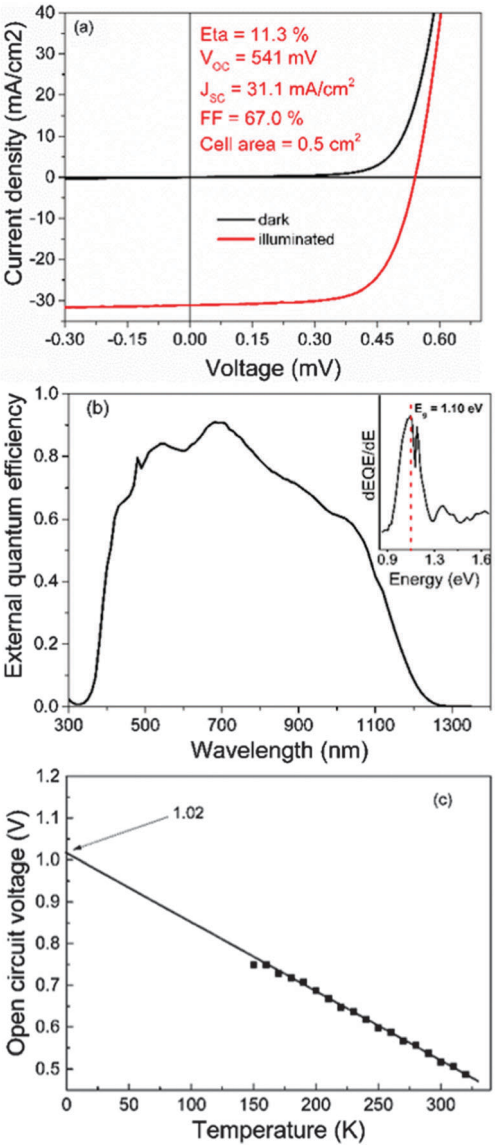

Fig. 5 (a) Current–voltage, (b) external quantum efficiency characteristics and (c) temperature dependent open circuit voltage of the 11.3% efficiency solar cell. The inset in (b) shows the differentiation of the external quantum efficiency *versus* the energy showing an estimation band gap at 1.10 eV.

EQE with the simulated ones, we can clearly see that the effective absorber thickness (large grained layer) is higher than that of the 250 nm one but slightly lower than that of the 500 nm thick simulated one. Note that the simulated EQE curves are from the one-dimensional calculation without considering grain boundary recombination and that the diffusion length was assumed to not limit carrier collection. These simplifications in the model can explain that the simulated 500 nm thick absorber still shows better red response than the actual cell.[39] These considerations suggest that by increasing the effective absorber thickness one should be able to increase the current density and efficiency of the cells.[40,41] Although the total thickness of the precursor can be simply increased by increasing the number of printing cycles as well as the printing resolutions, the thickness of the presumed active layer does not increase significantly when using the same annealing conditions. Fig. S3(a) (ESI†) shows that when the total CIGSSe thickness increases to 1.4 μm, the large grain layer is only slightly thicker (670 nm) while the fine grain layer thickness significantly increased to approximately 730 nm. While the current density of the device increased by around 2.1 mA cm^{-2} due to the slightly thicker active layer, the conversion efficiency of the device dropped to 9.5% due to the lower open circuit voltage and fill factor (Fig. S3(b), ESI†). This indicates that the preheating and annealing conditions (temperature, time, and chalcogen partial pressure) would have to be adapted for the thicker precursor in order to maintain the electronic properties and relative thickness of the large grain layer.[42–44] For example, Wang *et al.*[42] have investigated the influence of selenium pressure on the CIGSe grain grown from molecular precursors during selenization. They found that higher selenium vapour pressure helped to get larger CIGSe grains.

By integration of the EQE a current density of 32.4 mA cm^{-2} is derived, which is slightly higher than the value acquired by the current–voltage measurements, and is reasonable considering the grid shading of the device. The band gap estimated by the maximum value of the derivative of EQE over energy is estimated to be 1.10 eV, which is slightly lower than that in typical high efficiency cells. Fig. 5(c) shows the variation of open circuit voltage as a function of device temperature. The temperature dependent *J–V* characteristics of CIGSSe solar cells can be used as a tool to identify the dominant recombination mechanism, *i.e.*, bulk *vs.* interface recombination.[45–47] The extrapolated open circuit voltage at 0 K is 1.02 V. If we assume a thermally activated recombination process with an activation energy of 1.02 eV ($E = q^{*}V_{OC}$ (0 K)), this value is close enough to the absorber band gap estimated from EQE (1.10 eV) to justify the assumption that the cell efficiency is limited by the absorber bulk recombination rather than the hetero-interface. On the other hand, the small remaining discrepancy may indicate that there is potential for optimizing the band gap grading (originating from a higher sulphur content at the surface and a higher Ga content towards the back contact).

In summary, we reported on a low precursor wastage and cost-effective route for the fabrication of CIGSSe absorbers using a promising scalable inkjet printing technique. After reactive annealing, the CIGSSe absorber shows a layered structure with a large grained layer at the surface and a fine grained layer near the back contact. Ga was found to accumulate in the fine grained layer near the back contact. Solar cells with a total area efficiency exceeding 11% have been achieved. The poor infrared response in the EQE curve is probably caused by insufficient light absorption in the thin CIGSSe absorber layer. The band gap of the absorber is estimated to be 1.10 eV. The dominant recombination mechanism in the solar cell is the absorber bulk recombination. These encouraging results are a first indication that the unique advantages of air-stable inks and inkjet printing can be exploited without sacrificing device performance.

Experimental

The formation of the CIGSSe thin films includes four main steps as shown in Scheme 1. The first step is the formulation of a printable Cu–In–Ga ink by mixing the metal nitrate precursors in a solvent mixture of 2-propanol and ethylene glycol. Specifically, 0.87 g copper(II) nitrate trihydrate (Sigma-Aldrich, p.a. 99–104%,), 1.131 g indium nitrate hydrate (Sigma-Aldrich, 99.9%) and 0.394 g gallium nitrate hydrate (Sigma-Aldrich, 99.9%) were mixed with 5 mL 2-propanol (Sigma-Aldrich, 99.5%) and 4 mL anhydrous ethylene glycol (Sigma-Aldrich, 99.8%). The metal nitrates can be dissolved within a few minutes under ultrasonication, resulting in a clear blue ink as shown in Fig. 1(a). Note that the solvent of ethylene glycol utilized here serves two functions: on the one hand, it is used to adjust the viscosity of the precursor ink due to its high viscosity (16.1 cP) and, on the other hand, it is also used to prevent nozzle clogging due to its low vapor pressure.

The second step is inkjet printing of the formulated Cu–In–Ga ink onto the Mo coated soda lime glass substrate to form the precursor film. The printer used for printing is a PiXDRO LP50 printer from OTB Solar, Roth & Rau. A spectra print head (SE 128) with 128 piezoelectric nozzles is used for printing. The diameter of each nozzle is 35 μm. It should be noted that the drop volume could be tuned by adjusting printing parameters such as the voltage applied to the print head and the viscosity of the ink. In our experiment, the applied pulse voltage of the print head is between 75 and 85 V and the droplet volume is close to 15 pl (Fig. S1, ESI†). The printing speed was set to 200–300 mm s^{-1}. The resolutions in both the *X* and *Y* directions for the printing were between 320 and 400 dpi. The Mo coated soda lime glass substrate with a dimension of 10 cm × 10 cm is placed on the substrate table which is heated to 50 °C. The as-deposited Cu–In–Ga precursor thin films were baked on a pre-heated hot plate at 250 °C for 2 min after printing to remove the residual solvent. Based on the printing resolution and the droplet volume, the volume of ink needed for each printing on an inch by inch substrate is calculated to be less than 2.5 μL. To reach the desired thickness, the inkjet printing and pre-heating steps were repeated. After that, the precursor thin films were cut into 50 mm × 25 mm size and annealed under ambient pressure in a quartz tube furnace under a reactive atmosphere to allow the formation and crystal growth of the CIGSSe thin film absorbers. The annealing profile is shown in Scheme 1 in the fourth step. It should be noted that the quartz tube was evacuated and filled with argon three times before heating. Argon was flowed through the quartz tube during the whole annealing process. Prior to solar cell fabrication, the CIGSSe absorbers were soaked in 20–24% $(NH_4)_2S$ for 30 s and etched by 10% KCN for 3 min to remove potential $Cu_x(S,Se)$ phases.[48] Solar cells were fabricated by chemical bath deposition of a CdS buffer layer, and by sputtering of i-ZnO and aluminum doped ZnO window layers. A Ni/Al contact grid on top of the solar cell was deposited by evaporation using a shadow mask. Finally, solar cells with an area of 0.5 cm^2 were defined by mechanical scribing. No antireflection coating layer was applied.

Characterization

The contact angle was measured by using the ''contact angle system OCA'' obtained from Data Physics Instruments GmbH, Germany. Thermogravimetric analysis (TGA) was performed using a NETZSCH STA 409C apparatus under argon flow (100 ml min^{-1}) and at 10 °C min^{-1} ramp rate. The structure of the films was studied by grazing incident X-ray diffraction (GIXRD) and Raman spectroscopy. The GIXRD patterns were acquired in the 2θ range from 15 to 70° on a Bruker D8-Advance X-ray diffractometer with CuKα1 radiation at an incident angle of 5° using a step size of 0.02° and a step time of 5 seconds. For the Raman measurements a Dilor LabRam Raman setup was used. A HeNe laser with a wavelength of 632.8 nm was used as an excitation source. To avoid laser heating the beam power was kept below 7 mW. Raman spectra were recorded in a backscattering configuration using a microscope and a motorized XY stage. The micro-Raman spectroscopy with a 50× objective was performed at room temperature. Silicon was used as a reference for the calibration. The morphologies of the layers were analysed in a LEO 1530 GEMINI scanning electron microscope (SEM) of Zeiss. The SEM image was recorded at an acceleration voltage of 10 kV. Energy dispersive X-ray (EDX) spectroscopy analysis was performed under the LEO GEMINI 1530 field-emission gun scanning electron microscope (SEM) with an acceleration voltage of 20 kV and a Thermo Noran X-ray silicon drift detector (acquisition and evaluation software, Noran System Seven). Current–voltage (*I–V*) characteristics were analysed using an in-house class A sun simulator under standard test conditions (AM 1.5G, 100 mW cm^{-2} and 25 °C). Quantum efficiency analysis was performed using an illumination system including two sources (halogen and xenon lamps) and a Bentham TM300 monochromator (Bentham Instruments, Berkshire, UK). The reference measurements were performed on calibrated Si and Ge detectors. Temperature dependent *I–V* measurements on the best cells were carried out inside a cryostat which has a transparent window allowing the light to pass through. The samples were mounted on a hollowed steel stage which can be flooded with liquid nitrogen to cool down the sample. The temperature was detected by a thermocouple and adjusted by an electrical heater. During the measurement, the cryostat is maintained at a pressure of about 10^{-6} mbar using a turbo pump. The measuring temperature was in the range of 150–320 K in steps of 10 K. The sample is illuminated by LED arrays simulating the solar spectrum. Also, the light intensity used in this experiment is slightly lower than that of the standard sun simulator as indicated by the lower short circuit current density compared to that measured in the standard sun simulator.

Acknowledgements

The authors would like to thank C. Kaufmann for the supply of Mo substrates, and C. Ferber and M. Kirsch for the completion of the devices.

References

1 M. A. Green, K. Emery, Y. Hishikawa, W. Warta and E. D. Dunlop, *Prog. Photovolt.: Res. Appl.*, 2016, **24**, 3–11.

2 A. Chirila, S. Buecheler, F. Pianezzi, P. Bloesch, C. Gretener, A. R. Uhl, C. Fella, L. Kranz, J. Perrenoud, S. Seyrling, R. Verma, S. Nishiwaki, Y. E. Romanyuk, G. Bilger and A. N. Tiwari, *Nat. Mater.*, 2011, **10**, 857–861.
3 http://cigs-pv.net/.
4 P. Jackson, D. Hariskos, R. Wuerz, O. Kiowski, A. Bauer, T. M. Friedlmeier and M. Powalla, *Physica Status Solidi RRL: Rapid Research Letters*, 2015, **9**, 28–31.
5 http://www.solar-frontier.com/eng/news/2015/C051171.html.
6 H. Azimi, Y. Hou and C. J. Brabec, *Energy Environ. Sci.*, 2014, **7**, 1829–1849.
7 M. Singh, H. M. Haverinen, P. Dhagat and G. E. Jabbour, *Adv. Mater.*, 2010, **22**, 673–685.
8 S. E. Habas, H. A. S. Platt, M. F. A. M. van Hest and D. S. Ginley, *Chem. Rev.*, 2010, **110**, 6571–6594.
9 S. J. Park, H. S. Jeon, J. W. Cho, Y. J. Hwang, K. S. Park, H. S. Shim, J. K. Song, Y. Cho, D. W. Kim, J. Kim and B. K. Min, *ACS Appl. Mater. Interfaces*, 2015, **7**, 27391–27396.
10 D. Zhao, Q. Tian, Z. Zhou, G. Wang, Y. Meng, D. Kou, W. Zhou, D. Pan and S. Wu, *J. Mater. Chem. A*, 2015, **3**, 19263–19267.
11 T. K. Todorov, O. Gunawan, T. Gokmen and D. B. Mitzi, *Prog. Photovolt.: Res. Appl.*, 2013, **21**, 82–87.
12 A. R. Uhl, J. K. Katahara and H. W. Hillhouse, *Energy Environ. Sci.*, 2016, **9**, 130–134.
13 G. Wang, S. Wang, Y. Cui and D. Pan, *Chem. Mater.*, 2012, **24**, 3993–3997.
14 S. M. McLeod, C. J. Hages, N. J. Carter and R. Agrawal, *Prog. Photovolt.: Res. Appl.*, 2015, **23**, 1550–1556.
15 B.-S. Lee, Y. Hwang, H. N. Pham, J. Y. Kim, M. H. Song and D.-K. Lee, *J. Mater. Chem. A*, 2015, **3**, 15889–15896.
16 U. Berner, D. Colombara, J. de Wild, E. V. C. Robert, M. Schütze, F. Hergert, N. Valle, M. Widenmeyer and P. J. Dale, *Prog. Photovolt.: Res. Appl.*, 2016, **24**, 749–759.
17 U. Berner and M. Widenmeyer, *Prog. Photovolt.: Res. Appl.*, 2015, **23**, 1260–1266.
18 A. R. Uhl, C. Fella, A. Chirilă, M. R. Kaelin, L. Karvonen, A. Weidenkaff, C. N. Borca, D. Grolimund, Y. E. Romanyuk and A. N. Tiwari, *Prog. Photovolt.: Res. Appl.*, 2012, **20**, 526–533.
19 M. A. Hossain, Z. Tianliang, L. K. Keat, L. Xianglin, R. R. Prabhakar, S. K. Batabyal, S. G. Mhaisalkar and L. H. Wong, *J. Mater. Chem. A*, 2015, **3**, 4147–4154.
20 W. Septina, M. Kurihara, S. Ikeda, Y. Nakajima, T. Hirano, Y. Kawasaki, T. Harada and M. Matsumura, *ACS Appl. Mater. Interfaces*, 2015, **7**, 6472–6479.
21 M. A. Hossain, M. Wang and K. L. Choy, *ACS Appl. Mater. Interfaces*, 2015, **7**, 22497–22503.
22 B. A. Andersson, C. Azar, J. Holmberg and S. Karlsson, *Energy*, 1998, **23**, 407–411.
23 W. Wang, Y.-W. Su and C.-H. Chang, *Sol. Energy Mater. Sol. Cells*, 2011, **95**, 2616–2620.
24 X. Lin, J. Kavalakkatt, M. C. Lux-Steiner and A. Ennaoui, *Adv. Sci.*, 2015, **2**, 1500028.
25 L. Wang, X. Lin, A. Ennaoui, C. Wolf, M. C. Lux-Steiner and R. Klenk, *EPJ Photovoltaics*, 2016, **7**, 70303.
26 X. Lin, J. Kavalakkatt, N. Brusten, M. C. Lux-Steiner and A. Ennaoui, Inkjet printing of Kesterite and Chalcopyrite thin film absorbers for low cost photovoltaic application, *Proceedings of the 29th European Photovoltaic Solar Energy Conference and Exhibition*, Amsterdam, 2014, pp. 1876–1879.
27 J. Wang, L. Wang, Y. Song and L. Jiang, *J. Mater. Chem. C*, 2013, **1**, 6048.
28 D. Tian, Y. Song and L. Jiang, *Chem. Soc. Rev.*, 2013, **42**, 5184–5209.
29 D. G. Tuck, E. J. Woodhouse and P. Carty, *J. Chem. Soc. A*, 1966, 10771080.
30 K. H. Stern, *J. Phys. Chem. Ref. Data*, 1972, **1**, 747–772.
31 V. Berbenni, C. Milanese, G. Bruni and A. Marini, *J. Therm. Anal. Calorim.*, 2005, **82**, 401–407.
32 R. Bacewicz, W. Gqbicki and J. Filipowicz, *J. Phys.: Condens. Matter*, 1994, **6**, L777–L780.
33 I.-H. Choi, *Thin Solid Films*, 2011, **519**, 4390–4393.
34 X. Lin, J. Kavalakkatt, A. Ennaoui and M. C. Lux-Steiner, *Sol. Energy Mater. Sol. Cells*, 2015, **132**, 221–229.
35 W. Wu, Y. Cao, J. V. Caspar, Q. Guo, L. K. Johnson, I. Malajovich, H. D. Rosenfeld and K. R. Choudhury, *J. Mater. Chem. C*, 2014, **2**, 3777.
36 S. Rehan, K. Y. Kim, J. Han, Y. J. Eo, J. Gwak, S. K. Ahn, J. H. Yun, K. Yoon, A. Cho and S. Ahn, *ACS Appl. Mater. Interfaces*, 2016, **8**, 5261–5272.
37 R. Klenk and H. W. Schock, Photocurrent Collection in Thin Film Solar Cells - Calculation and Characterization for $CuGaSe_2$/(Zn,Cd)S, *Proceedings of the 12th European Photovoltaic Solar Energy Conference and Exhibition*, Amsterdam, 1994, pp. 1588–1591.
38 M. Burgelman, P. Nollet and S. Degrave, *Thin Solid Films*, 2000, **361–362**, 527–532.
39 S. Harndt, C. A. Kaufmann, M. C. Lux-Steiner, R. Klenk and R. Nürnberg, *EPJ Photovoltaics*, 2015, **6**, 60101.
40 E. Jarzembowski, M. Maiberg, F. Obereigner, K. Kaufmann, S. Krause and R. Scheer, *Thin Solid Films*, 2015, **576**, 75–80.
41 O. Lundberg, M. Bodegård, J. Malmström and L. Stolt, *Prog. Photovolt.: Res. Appl.*, 2003, **11**, 77–88.
42 W. Wang, S. Y. Han, S. J. Sung, D. H. Kim and C. H. Chang, *Phys. Chem. Chem. Phys.*, 2012, **14**, 11154–11159.
43 C. K. Miskin, W.-C. Yang, C. J. Hages, N. J. Carter, C. S. Joglekar, E. A. Stach and R. Agrawal, *Prog. Photovolt.: Res. Appl.*, 2015, **23**, 654–659.
44 Y. Qu, G. Zoppi and N. S. Beattie, *Sol. Energy Mater. Sol. Cells*, 2015, DOI: 10.1016/j.solmat.2015.12.016.
45 Q. Cao, O. Gunawan, M. Copel, K. B. Reuter, S. J. Chey, V. R. Deline and D. B. Mitzi, *Adv. Energy Mater.*, 2011, **1**, 845–853.
46 S. S. Hegedus and W. N. Shafarman, *Prog. Photovolt.: Res. Appl.*, 2004, **12**, 155–176.
47 M. Turcu, O. Pakma and U. Rau, *Appl. Phys. Lett.*, 2002, **80**, 2598.
48 M. Buffière, A.-A. E. Mel, N. Lenaers, G. Brammertz, A. E. Zaghi, M. Meuris and J. Poortmans, *Adv. Energy Mater.*, 2015, **5**, 1401689.